International Journal of Pharmaceutics 418 (2011) 273–285

Contents lists available at ScienceDirect

International Journal of Pharmaceutics

journal homepage: www.elsevier.com/locate/ijpharm

Modeling and simulation of compact strength due to particle bonding using a hybrid discrete-continuum approach

A. Koynov, I. Akseli, A.M. Cuitiño*

[a] Rutgers, The State University of New Jersey, Department of Mechanical and Aerospace Engineering, Piscataway, NJ 08854, USA

ARTICLE INFO

Article history:
Received 5 January 2011
Received in revised form 7 May 2011
Accepted 1 June 2011
Available online 28 June 2011

ABSTRACT

The compaction of powder beds into solid bodies occurs by virtue of the formation of inter-particle bonds. The mechanical strength of the compact depends on the type of bonding interaction, as well as, the inter-particle contact area created in the compression process. A hybrid quasi-continuum computational approach has been implemented to study the bonding occurring in compressed granular assemblies. The approach resolves the powder bed on the particle level, allowing for the tracking of contact area generated by particle deformation and the computation of history-dependent inter-particle bonding forces. The magnitude of the bonding force is calculated using a synthetically constructed potential aiming to mimic the shape of typical molecular-type interactions. The uniaxial compaction and subsequent relaxation of powder beds, representative of pharmaceutical excipients have been simulated. Due to the bonding occurring between the individual particles the compressed beds acquire tensile strength. Post-relaxation tensile loading of the compacts is used to quantify the magnitude of this tensile strength. To validate the computational results, tablets are prepared using a compaction simulator under conditions closely resembling the simulated scenarios, where subsequently the tablets are subjected to tensile loads until failure. The predicted values for the tablet strength utilizing the present methodology capture the general trends exhibited by the experimental record.

1. Introduction

A typical tableting process can be tentatively divided into several stages following the progressively increasing axial compressive load on the powder bed. In the rearrangement stage, the powder bed is densified by virtue of the translational and rotational motion of individual particles filling in the void structures created during die-filling due to cohesive forces and geometric interference. Once the bed is compacted to the point where no significant non-affine motion of individual particles is occurring, further loading results in the elastic and, upon yielding, subsequent plastic deformation (and if applicable fragmentation) of the particles. It is during this stage that the powder bed is transformed into a solid body through the bonding of the individual particles to each other. Despite the importance of mechanical strength for tablet stability, integrity during transportation and storage, as well as disintegration properties, the phenomena controlling bond formation during compaction are still poorly understood and process design is based mostly on trial and error.

Depending on the nature of the compacted materials particle bonding can occur through a variety of mechanisms. Typically, these mechanisms are distinguished based on the nature of the bonding force. Electrostatic bonding can occur due the accumulation of triboelectric charge in the powder bed or because of the presence of polar functional groups on the particles surface. Molecular force bonding, while technically also driven by electrostatic interactions is recognized as a separate mechanism due to the large difference in separation scales, at which the two phenomena manifest. Caused by van der Waals type interactions between charged or polarized molecules, molecular force bonding requires the powder particles to be in extremely close contact. In the presence of humidity, liquid menisci can form between particles leading to attractive forces proportional to the surface tension of the liquid. Finally, during prolonged contact between particles, solid bridges can form due to material melting, self-diffusion of atoms and recrystallization.

For most typical pharmaceutical excipients, bonding is believed to only occur by virtue of molecular forces and the formation of solid bridges. Several experimental techniques have been developed to asses the contribution of the two potential mechanisms towards the development of mechanical strength in pharmaceutical compacts. In the case of electrically-conductive materials, resistivity measurements can be used to detect the formation of solid bridges (Bhatia and Lordi, 1979). The ratio between tablet strength and the surface area available in the initial powder bed can be used to discriminate between solids held together by liquid bridges and molecular forces (with the latter being orders of magnitude weaker

* Corresponding author.
E-mail address: cuitino@jove.rutgers.edu (A.M. Cuitiño).

0378-5173/$ – see front matter © 2011 Elsevier B.V. All rights reserved.
doi:10.1016/j.ijpharm.2011.06.006

and hence yielding much lower surface-specific strengths). The use of lubricant films can also help differentiate between the two potential mechanisms. While a film of magnesium stearate will significantly decrease the molecular attractive forces between two particles (Boer et al., 1978; Vromans and Lerk, 1988), the high local stresses associated with the formation of solid bridges will facilitate the penetration of the lubricant layer and will diminish its effect on the strength of the bond (Zuurman et al., 1999). Since van der Waals forces are inversely proportional to the dielectric constant of the medium, compaction of tablets in different fluids and the comparison of their mechanical strength with ones compacted in air can also help identify the contribution of molecular forces to the bonding of the powder bed (Olsson et al., 1996; sa Adolfsson et al., 1997). While the above methods have contributed a great deal to the understanding of the phenomena underlying the formation of solids during powder compaction, they offer no quantitative predictive capabilities as far as the post-compaction mechanical properties of the granular bed. A proper estimate of the mechanical strength of a compacted solid is contingent upon the knowledge of the amount of inter-particle contact area created during the plastic deformation stage of the compression. A coupling between a modeling tool capable of capturing the local deformations occurring during the densification of the bed and a bonding force formulation consistent with the physical inter-particle interactions is, therefore, necessary to adequately apply quality by design to the process of powder compaction.

Early efforts in the modeling of powder compaction consisted of models correlating relative density and applied pressure via first order "rate-like" expressions (Heckel, 1961; Kawakita and Ludde, 1970). Subsequent empirical models were predicated on the assumption that the behavior of the powder bed can be approximated by a continuum with an appropriate constitutive model (Cocks and Sinka, 2007). The methods consist of solving the conservation equations for mass, energy and momentum, coupled with constitutive laws, such as those describing stress–strain relations and die wall friction. Powders are treated as elastic-plastic materials with their yield behavior modeled using yield surfaces. Early versions assumed a Green/Shima type yield surface (Shima and Oyane, 1976; Kuhn and Downey, 1973), a quadratic function of the von Mises effective stress. These models described the state of the compact in terms of its porosity with equivalent values for the yield stress in tension as well as compression. The last several decades have been marked by the transition towards models originating from soil mechanics simulation such as Cam-Clay (Schofield and Wroth, 1968; Borja and Lee, 1990), DiMaggio–Sandler (DiMaggio and Sandler, 1971) and Drucker–Prager (Drucker and Prager, 1952). Experimentally calibrated (Pavier and Doremus, 1999), these models are fairly accurate in the prediction of the densification of the powder beds (also based on the evolution of a single variable, such as the relative density), however, they do not explicitly resolve inter-particle bonding. Continuum models for granular materials that account for tensile strength, *e.g.* (Dvorkin et al., 1989), require ad hoc calibration of the parameters describing that regime.

Of the above, the Drucker–Prager Cap model has gained the highest popularity as far as the modeling of pharmaceutical tablet compaction is considered (Aydin et al., 1996; Michrafy et al., 2002; Dec et al., 2003; Sinka et al., 2003; Kadiri et al., 2005; Wu et al., 2005; Sinha et al., 2010). Recently the FEM method has been extended (Khoei et al., 2006), enabling it to handle cracks and discontinuities. Despite their success in reproducing the densification of a compressed powder, yield surface Finite Element Methods have the disadvantage of requiring experimental data for the calibration of their parameters.

Micro-mechanical models, such as the one developed by (Fleck et al., 1992) aim to simulate the macroscopic compaction behavior based on the resolution of the motion of individual particles in a random close packing with visco-plastic dissipation occurring at the points of contact. The model only considers the affine motion of particles as caused by the macroscopic strain. In the original implementation the model assumed assume fully sticking contacts, with the material having as much strength in hydrostatic tension as in hydrostatic compression. Subsequent iterations included different contact strengths in tension and compression (Fleck, 1995) as well as the addition of different contact laws (Fleck et al., 1997)derived from the mutual indentation of dissimilar particles (Storakers et al., 1999). These methods are usually limited to stage I compression (characterized by interconnected pores between the particles, with plastic flow at the zones of inter-particle contact and no interaction between such zones). Stage II compaction, where the pores close are usually approached using models developed for the study of ductile fracture and metallurgical powder compaction such as Gurson (1977).

Following the above work, among others, (Redanz and Fleck, 2001) formulated a DEM model aiming to explore the non-affine motion of particles, such as sliding and rolling. In general, DEM models have recently enjoyed significant success in reproducing the behavior of powder beds during shearing (Thornton and Antony, 2000; Oda and Iwashita, 2000) and compaction (Heyliger and McMeeking, 2001; Martin and Bouvard, 2003; Pizette et al., 2010). Recent contributions by Procopio and Zavaliangos (2005); Jerier et al. (2011) present DEM formulations combined with the full FEM discretization of the individual particles.

Prediction of the strength of powder compacts requires the resolution of the bonding forces between the individual particles. Early contributions in the study of adhesive contacts between elastic particles came courtesy of Johnson et al. (1971), usually referred to as the JKR model and (Derjaguin et al., 1975) DMT model. Both model assumed spherical particles. The JKR model predicts a deformation of the sphere, caused by the adhesive forces, results in the formation of a neck at the point of contact, where all interfacial forces are confined. Conversely, the DMT model disregards deformation caused by adhesion and only considers that resulting from the Hertzian force distribution, with adhesive forces acting outside the contact zone. The disagreement between the two models was resolved by Tabor (1977) who showed that each applies to a specific limiting case (large, soft particles for JKR and small rigid ones for DMT). Tabor also introduced a dimensionless parameter to use to gauge the applicability of each model for particular cases. Muller et al. (1980) provided the first solution for the adhesion of elastic spheres for an intermediate case, coupling the Lennard–Jones potential for the description of the surface force and the Boussinesq elastic solution for a concentrated force for the resolution of the interfacial deformation. Efforts to solve the problem of elastic adhesive contact analytically have resulted in the MD model (Maugis, 1992), which covers the entire range of contact properties. Both the JKR and DMT models have been subsequently extended to consider plastic deformation as well (Maugis and Pollock, 1984 and Chang et al., 1987, respectively). Following numerical implementations of higher accuracy included the works of Kogut and Etsion (2003); Song and Srolovitz (2006); Gilabert et al. (2007); Kadin et al. (2008) among others.

The aim of this article is to apply a quasi-continuum formulation for the simulation inter-particle bonding in granular systems. First proposed for the study of the interactions between cracks, grain boundaries and dislocations in metallic crystals, quasi-continuum methods have also been used to simulate the formation and annihilation of Lomer–Cottrell junctions in fcc single crystals (Rodney and Phillips, 1999), and more recently to analyze dislocation nucleation and metallic phase transformation during indentation (Shenoy et al., 2000; Smith et al., 2000). For the purposes of this work, the quasi-continuum approach has been implemented in a way suitable for the description of granular systems composed of a large

number of particles of different sizes and materials. Results for powder compaction of mixtures of different materials have previously been published by Zheng and Cuitino (2002) The approach relies on the assumption that the particle displacements are small enough that they can be described by means of a constrained field—provided by a typical FEM mesh. The formulation, described in detail in Section 2, is derived specifically for quasi-static processes, however the extension to include dynamic conditions is straightforward. The model is based on the principle of virtual displacements and, for reversible systems, it can be recast as a variational problem. An interpolation scheme is proposed in Section 3 for resolving the non-local interactions between particles contained in different mesh cells in a local manner. This procedure renders *s*ymmetric local stiffness matrices, which is consistent with systems where a potential energy can be defined.

The reason the quasi-continuum method is particularly well suited for the study of powder compaction is that, on one hand, being an FEM method, it is capable of providing "fast" simulations of the behavior of the entire bed, as described by the density distribution, for example. On the other hand, since individual particle information is stored and updated at all times, it is capable of computing yield behavior explicitly by resolving individual particle–particle interactions. The formulation is implemented for 3D cases involving cohesive particles of different sizes. The resolution of the inter-particle bonding eschews the detailed adhesive contact models described above in favor of a simple geometric estimation of the interfacial area. This is done for the purposes of reduction of computational time and resources. An example showing the compaction, relaxation and subsequent tensile loading of Avicel PH102 is presented in Section 4. The initial configuration is generated by a ballistic deposition technique (Jullien and Meakin, 1989; Westwood, 1989). The evolution of the macroscopic load–displacement profiles as well as the spatial density and stress distribution are recorded. The tensile strength of the simulated compacted solids is compared to experimental results to obtain a reasonably close fit.

2. General formulation

Consider a finite set of *P* spherical particles, $\mathcal{P}$, which is subjected to a discrete applied force field given by

$$\mathbf{f}^m \quad \forall m \in \mathcal{P} \tag{1}$$

Also consider that an interaction potential exists for each element (particle) pair in the set $\mathcal{P}$,

$$w^{mn}(r^{mn}) \quad \forall (m,n) \in \mathcal{P}, \tag{2}$$

where r^{mn} denotes the current distance between the centers of particles m and n. This distance r^{mn} can be easily computed in terms of the current positions $\mathbf{x}^m$ and $\mathbf{x}^n$ of the particles m and n, respectively, then

$$r^{mn} = \left(\mathbf{r}^{mn} \cdot \mathbf{r}^{mn}\right)^{1/2} \tag{3}$$

where $\mathbf{r}^{mn}$ is the current vector position of particle m respect to n, defined as

$$\mathbf{r}^{mn} = \mathbf{x}^m - \mathbf{x}^n. \tag{4}$$

The current position can be expressed by,

$$\mathbf{x}^m = \mathbf{X}^m + \mathbf{u}^m, \tag{5}$$

where $\mathbf{X}^m$ and $\mathbf{u}^m$ are the reference location and the discrete displacement field of each particle $m \in \mathcal{P}$, respectively.

Using the previous equations, the current distance between particles can be expressed as

$$r^{mn} = \left[(R^{mn})^2 + 2\mathbf{R}^{mn} \cdot \mathbf{u}^{mn} + \mathbf{u}^{mn} \cdot \mathbf{u}^{mn}\right]^{1/2} \tag{6}$$

where,

$$R^{mn} = \left(\mathbf{R}^{mn} \cdot \mathbf{R}^{mn}\right)^{1/2} \text{ Initial distance between particles } m \text{ and } n \tag{7}$$

$$\mathbf{R}^{mn} = \mathbf{X}^m - \mathbf{X}^n \text{ Reference position of particle } m \text{ respect to } n \tag{8}$$

$$\mathbf{u}^{mn} = \mathbf{u}^m - \mathbf{u}^n \text{ Relative displacement of particle } m \text{ respect to } n \tag{9}$$

2.1. Principle of virtual work

The equilibrium condition of the set of P particles, $\mathcal{P}$, can be enforced weakly by means of the principle of virtual work,

$$\frac{1}{2}\sum_{\forall m \in \mathcal{P}}\sum_{\forall n \in \mathcal{V}_m} \delta w^{mn} + \sum_{\forall m \in \mathcal{P}} \mathbf{f}^m \cdot \delta \mathbf{u}^m = 0 \tag{10}$$

where δw^{mn} is the variation of the interaction potential of the pair (m,n) due to a variation of the discrete displacement field $\mathbf{u}^m$ and $\mathcal{V}_m$ is the set of the neighbors of the particle m, which can be expressed as

$$\mathcal{P} \supseteq \mathcal{V}_m = \{n | n \in \mathcal{P} \quad \text{and} \quad r^{mn} \le l_{\max}\} \tag{11}$$

Here $l_{\max}$ is a cut-off distance. The variation of the potential is given by

$$\delta w^{mn} = \frac{\mathrm{d}w^{mn}}{\mathrm{d}r^{mn}} \delta r^{mn} = \frac{\mathrm{d}w^{mn}}{\mathrm{d}r^{mn}} \frac{\partial r^{mn}}{\partial \mathbf{u}^{mn}} \cdot \delta \mathbf{u}^{mn}, \tag{12}$$

and noticing that

$$\frac{\partial r^{mn}}{\partial \mathbf{u}^{mn}} = \frac{1}{r^{mn}}\left(\mathbf{R}^{mn} + \mathbf{u}^{mn}\right) = \frac{\mathbf{r}^{mn}}{r^{mn}} = \mathbf{e}^{mn} \tag{13}$$

Eq. (10) can be recast as

$$\frac{1}{2}\sum_{\forall m \in \mathcal{P}}\sum_{\forall n \in \mathcal{P}/n \neq m} \frac{\mathrm{d}w^{mn}}{\mathrm{d}r^{mn}} \mathbf{e}^{mn} \cdot \delta \mathbf{u}^{mn} + \mathbf{f}^m \cdot \delta \mathbf{u}^m = 0. \tag{14}$$

where $\mathbf{e}^{mn}$ is the unit vector in defining the direction from particle n to particle m. Furthermore, since

$$\frac{\mathrm{d}w^{mn}}{\mathrm{d}r^{mn}} = \frac{\mathrm{d}w^{nm}}{\mathrm{d}r^{nm}}, \tag{15}$$

$$\mathbf{e}^{mn} = -\mathbf{e}^{nm} \quad \text{and} \tag{16}$$

$$\mathbf{u}^{mn} = -\mathbf{u}^{nm}; \tag{17}$$

Eq. (14) yields

$$\sum_{\forall m \in \mathcal{P}} \left[\sum_{\forall n \in \mathcal{V}_m} \frac{\mathrm{d}w^{mn}}{\mathrm{d}r^{mn}} \mathbf{e}^{mn} + \mathbf{f}^m\right] \cdot \delta \mathbf{u}^m = 0. \tag{18}$$

Since $\delta \mathbf{u}^m$ is an arbitrary variation of the displacement field, the following condition has to be satisfied for every $m \in \mathcal{P}$

$$\left[\sum_{\forall n \in \mathcal{P}_m} \frac{\mathrm{d}w^{mn}}{\mathrm{d}r^{mn}} \mathbf{e}^{mn} + \mathbf{f}^m\right] = 0, \tag{19}$$

which is the equilibrium equation corresponding to particle m in order to satisfy Eq. (18). Since $\mathbf{e}^{mn}$ is the direction vector of the force,

it follows from Eq. (19) that the resultant force on particle m equals zero. Here dw^{mn}/dr^{mn} represents the magnitude of the interaction force between particles m and n.

2.2. Discretization

Consider a discretization of the domain Ω containing all the particles in the system into element domains Ω_e with $e = 1, \ldots, M$ such that $\Omega = \cap_e \Omega_e$ and with nodal points a ($a = 1, \ldots, nodes$).

An approximate solution to the weak equilibrium condition expressed in Eq. (18) can be attained by imposing a constrained displacement field, constructed as

$$\mathbf{u}^m = \sum_{\forall a} N_a^m \mathbf{U}_a \quad \text{and} \tag{20}$$

$$\mathbf{u}^{mn} = \sum_{\forall a} \left(N_a^m - N_a^n\right) \mathbf{U}_a = \sum_{\forall a} B_a^{mn} \mathbf{U}_a \tag{21}$$

where $\mathbf{U}_a$ is the displacement vector of the node a and N_a^m is the interpolation function which relates the displacement vector of particle m with the displacement vector of node a. Substituting Eq. (21) into Eq. (18) results in

$$\sum_{\forall a} \left\{ \sum_{\forall m \in \mathcal{P}} \left[\sum_{\forall n \in \mathcal{V}_m} \frac{1}{2} \frac{dw^{mn}}{dr^{mn}} \mathbf{e}^{mn} B_a^{mn} + \mathbf{f}^m N_a^m \right] \right\} \delta \mathbf{U}_a = 0, \tag{22}$$

which yields the following system of $d \times nodes$ nonlinear equations

$$\sum_{\forall m \in \mathcal{P}} \left[\sum_{\forall n \in \mathcal{V}_m} \frac{1}{2} \frac{dw^{mn}}{dr^{mn}} \mathbf{e}^{mn} B_a^{mn} + \mathbf{f}^m N_a^m \right] = 0 \quad \forall a = 1, \ldots, nodes \tag{23}$$

due to the arbitrary manner in which the $\delta \mathbf{U}_a$ can be selected (here d is the dimension of the space). Furthermore, considering the partition of the domain Ω, we can rewrite the previous equation as

$$\sum_{\forall e} \left\{ \sum_{\forall m \in \mathcal{P}_e} \left[\sum_{\forall n \in \mathcal{V}_m} \frac{1}{2} \frac{dw^{mn}}{dr^{mn}} \mathbf{e}^{mn} B_a^{mn} + \mathbf{f}^m N_a^m \right] \right\} = 0 \quad \forall a = 1, \ldots, nodes \tag{24}$$

where,

$$\mathcal{P} \supset \mathcal{P}_e = \left\{ \frac{m}{m \in \mathcal{P}} \quad \text{and } m \text{ is contained in the domain } \Omega_e \right\} \tag{25}$$

The above equality is a statement of the discrete equilibrium at the nodal points. Since the enforcement of this equality requires an iterative procedure, Eq. (24) is rewritten in indicial notation for the subsequent derivation of the tangent operator.

$$G_{ia}(\mathbf{U}) = \sum_{\forall e} \left\{ \sum_{\forall m \in \mathcal{P}_e} \left[\sum_{\forall n \in \mathcal{V}_m} \frac{1}{2} \frac{dw^{mn}}{dr^{mn}} e_i^{mn} B_a^{mn} + f_i^m N_a^m \right] \right\} = 0. \quad \forall a = 1, \ldots, nodes \quad \text{and} \quad \forall i = 1, d \tag{26}$$

Here G_{ia} represents the $d \times nodes$ equations which depend on the current position of the particles and thus on the discrete displacement field $\mathbf{U}$. In term of these nodal displacements, the Cartesian components of the current relative position vector $\mathbf{r}^{mn}$ can be then expressed by

$$r_i^{mn} = R_i^{mn} + \left(N_b^m - N_b^n\right) U_{ib} = R_i^{mn} + B_b^{mn} U_{ib}. \tag{27}$$

2.3. Tangent modulus

Next, we turn our attention to the derivation of the tangent modulus. Proper computation of this modulus is of importance in many cases. Examples include the preservation of convergence properties of nonlinear systems, such as the one described by Eq. (27) when direct methods such as Newton's are used; preconditioning in implementations where indirect methods are used; and assessment of the loss of ellipticity of the system. It can also be used to find approximate solutions of the time (or load) evolution of the constrained displacement field when explicit time-integration schemes such as forward gradients are considered.

By definition the tangent modulus is given by

$$K_{iajb} = \frac{\partial G_{ia}}{\partial U_{jb}} \tag{28}$$

Lengthly but straightforward derivation yields the following expression for the tangent operator

$$K_{iajb} = \sum_{\forall e} K_{iajb}^e = \sum_{\forall e} \left[\sum_{\forall m \in \mathcal{P}_e} \sum_{\forall n \in \mathcal{V}_m} B_a^{mn} B_b^{mn} \mathcal{A}_{ij}^{mn} \right] \tag{29}$$

where K_{iajb}^e is the elemental stiffness matrix and

$$\mathcal{A}_{ij}^{mn} = \frac{1}{2(r^{mn})^2} \left[\frac{d^2 w^{mn}}{(dr^{mn})^2} r_i^{mn} r_j^{mn} + \frac{1}{r^{mn}} \frac{dw^{mn}}{dr^{mn}} \langle \delta_{ij} r_s^{mn} r_s^{mn} - r_i^{mn} r_j^{mn} \rangle \right] \tag{30}$$

3. Local and nonlocal formulations

It is noteworthy that the above formulation is non-local since the neighbors of a given particle m contained in a given element e may be outside of the domain Ω_e. In systems, where long-range interactions dominate, the interaction distance may span several elements, necessitating the use of a non-local implementation. In systems dominated by short-range interaction (such as those governed by mechanical contact), on the other hand, a local formulation can provide a satisfactory approximation. To differentiate between local and non-local formulations, the following nomenclature is introduced for the shape functions $\mathbf{N}$. ${}^m\mathbf{N}_a^m$ is the interpolation function for particle m and node a computed for the element e which contains m, while ${}^n\mathbf{N}_a^m$ is the extrapolation function for particle m and node a computed for the element e which contains n. Notice that in general ${}^n\mathbf{N}_a^m \neq {}^m\mathbf{N}_a^n$.

The B matrix can then be written as

$$B_b^{mn} = \begin{cases} {}^m\mathbf{N}_b^m - {}^n\mathbf{N}_b^n & \text{for the } \textit{non-local} \text{ formaultion and} \\ {}^m\mathbf{N}_b^m - {}^m\mathbf{N}_b^n & \text{for the } \textit{local} \text{ formaultion} \end{cases} \tag{31}$$

The local formulation allows the evaluation of the contribution from each element independently, and is therefore amenable to implementation in conventional or local finite element codes. It can also be shown by direct substitution of Eq. (31) into Eq. (30) that the local formulation renders *symmetric* elemental stiffness matrices in the sense that

$$K_{iajb}^e = K_{jbia}^e. \tag{32}$$

The proposed computation of the interpolation functions for local formulations implies that the relative displacement between two particles belonging to different elements is computed once for each element, which in general yields a different result. The displacement of the particle lying outside of the element under consideration is *extrapolated* using the interpolation function of that particular element. The difference between computing the relative

displacements of particles residing in contiguous elements using a non-local approach (providing a unique relative displacement consistent with the deriving principle of virtual displacement) and a local approach can be estimated for linear interpolation functions by

$$\mathbf{u}^{mn}_{\text{nonlocal}} = \mathbf{u}^{mn}_{\text{local}} + \mathbf{C}(\eta_m + \eta_n) \tag{33}$$

where η_m and η_n are the distance from particles m and n to the shared element boundary respectively and $\mathbf{C}$ is a constant for the given set of elements. Thus, as long as the interacting particles in different elements remain close to the boundary, $\eta_m + \eta_n \to 0$, both methods yield similar relative displacements, $\mathbf{u}^{mn}_{\text{nonlocal}} \to \mathbf{u}^{mn}_{\text{local}}$. Since we are concerned with the compaction of particle systems, the local approach is implemented in this article.

4. Numerical simulations

4.1. Generation of the granular bed

The first step towards the simulation of the compaction of powder beds is the generation of the initial bed packing. Depending on the needs of the specific numerical experiment, these can be analytically produced regular arrangements or random structures obtained from a variety of sources, both numerical (such as DEM) and experimental (X-ray tomography). The simulation of the compaction of realistic granular beds requires the generation of a random initial packing, which resembles those found in nature. While any procedure, resulting in such an initial configuration could be applied successfully, for this work, an approach characterized by very short bed generation times was chosen. Granular beds can be effectively characterized through the qualification of their void space distribution. Void spaces belong to either of two general categories – intrinsic (due to the spherical or irregular shape of particles) and removable (caused by particle cohesion and characterized by meta-stable structures, which can be eliminated by particle rearrangement). In order to generate such packings, a ballistic deposition technique (Jullien and Meakin, 1988) has been implemented, in which particles, released sequentially from the top of the computational domain, are allowed to settle based on a set of simple rules. A particle is allowed to roll down other particles that it encounters until it is locked into a stable configuration. The basis of this approach is the stabilizing effect of center-to-center cohesive forces. In this context, cohesion is assumed to be strong enough to stabilize a particle both during deposition and afterwards, but remains otherwise undetermined. The mean densities obtained from this technique is generally lower than those obtained from models in which a cooperative reorganization of the particles is allowed to occur. In addition, powder beds generated using ballistic deposition exhibit vertical directionality not always present in materials with low cohesivity. However, for the purposes of the current study the method has been deemed adequate in generating beds resembling, in structure, those observed in reality – cohesive aggregates exhibiting large open structures due to the limited capacity for particle accommodation (Gioia et al., 2002; Redanz and Fleck, 2001). While the present study is focused on the bonding process during compaction, the quasi-continuum methodology allows to incorporate ordered/disordered packing states as generated for example by fully resolved DEM simulations of the pouring process. Such studies would further contribute to the understanding of the impact of filling on the properties of the compacts.

Fig. 1(a) shows a granular bed, numerically generated by pouring powder consisting of a single type of particles vertically into a frictionless container with a circular cross-section with a radius of 3 mm and a height of 5 mm. The shape of the particles is assumed to be spherical while their size (diameter) follows the distribution shown in Fig. 1(b). The density of the particle material is $\rho_s = 1.6\,\text{g/cm}^3$ and 34 mg of granules are poured into the container to form the bed. The initial relative density of the bed is 0.48. The particle size distribution, as well as all other particle properties in this work have been chosen to match those of Avicel PH102—a popular pharmaceutical excipient. The asymmetricity in the distribution (observed in real systems (Zhang and Chakrabarti, 2003) for example) has been obtained by overlapping two mono-modal distributions—one with a peak at 100 μ s and one with a peak at 50 μs. During the process of ballistic deposition, each particle, upon generation, is assigned a random radius with a probability following the above distribution.

To remove open structures, powder beds are usually stirred or shaken. One way to replicate this process numerically is by using discrete methods, solving the dynamic equations for each particle. However, as it was discussed in the introduction, such methods are too computationally expensive to be applied for large powder beds. Instead, a different method has been implemented, simulating the particle rearrangement due to the quasi-static motion of a top punch (Gioia et al., 2002). After each punch displacement step, particles are allowed to relax into a new non-deformed configuration. Fig. 2(a) shows the bed after a slight rearrangement. The relative bulk density at this point is 0.545. Further motion of the punch produces the bed seen in Fig. 2(b), with a relative bulk density of 0.576 and eventually the bed shown in Fig. 2(c) of a relative bulk density of 0.611. A better visualization of the shape of the initial void structures and their closing by particle rearrangement (along with an explanation of the closing mechanism) can be found in Gioia et al. (2002).

5. Local constitutive laws

A very attractive feature of the granular quasi-continuum approach is that specialized inter-particle laws can be readily incorporated into the formulation to account for effects such as plasticity, fracture and strain-rate dependency. Local or inter-particle laws should be provided to replicate the collective mechanical behavior of the system. The form of the law itself is a very complicated issue and its derivation is still an active research area in the literature. Large particle deformation, breakage and the potential penetration of one particle into another are all sources of additional difficulty. The laws can be extracted directly from experimental testing for some simple scenarios. This approach, however, is not feasible for systems composed of multiple materials with multiple particle sizes. Instead, theoretical models have been used, which despite offering but an approximation of the actual physical situation, can be easily applied for the study of complex systems. For the purposes of simplification, the local inter-particle interactions between two spherical particles are modeled separately in the five different regimes: (i) elastic contact, (ii) elastic–plastic contact, (iii) fully plastic, (iv) finite deformation and (v) tensile loading. While continuity of the interaction forces is required at transition points from one regime to the next, the continuity of their derivatives (stiffnesses) is not. This finite jump in the stiffness bears no consequences on either the energetics of the system or on the robustness of the numerical scheme.

Consider a binary interaction between particle m and n with radii r_m and r_n, Young's moduli E_m and E_n, Poisson's ratios ν_m and ν_n, and yielding stresses σ_{ym} and σ_{yn}, respectively. If the central distance between them is denoted by r^{mn}, the penetration distance is therefore expressed as $\Delta^{mn} = r_m + r_n - r^{mn}$ as shown in Fig. 3. Here Δ^{mn} can be positive or negative. The negative value implies the separation of one particle from the other when tension needs to be considered.

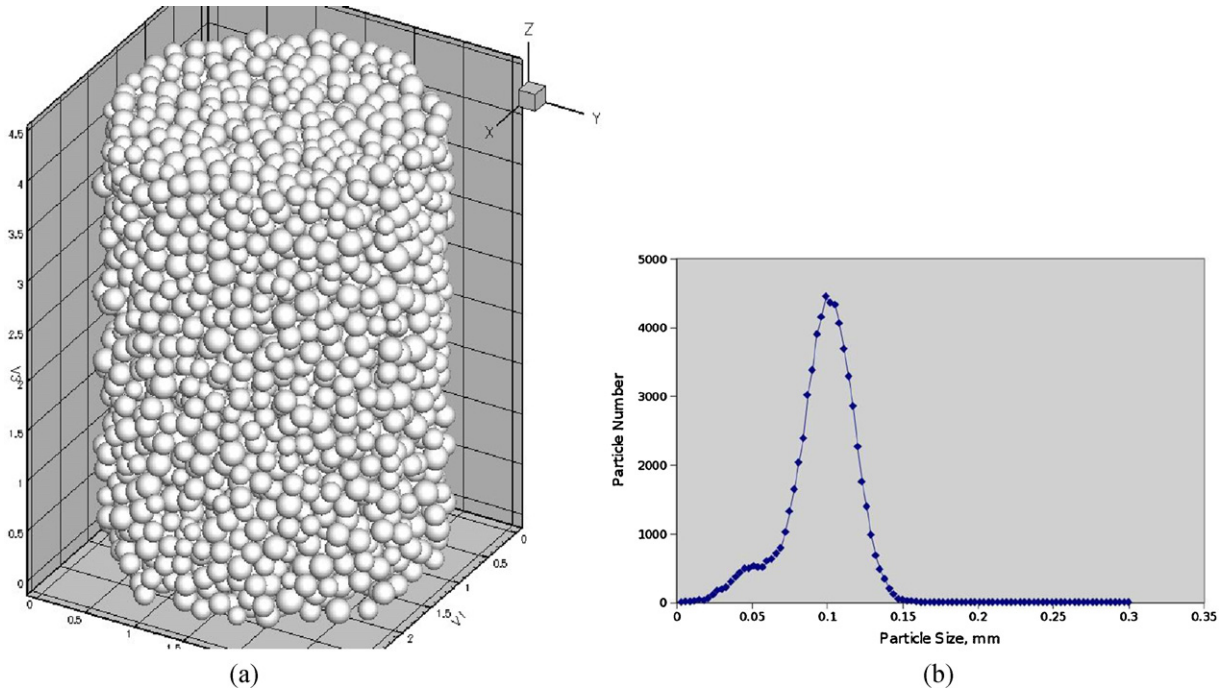

Fig. 1. (a) The initial granular bed after the powder is poured into a frictionless container with a circular cross-section with a radius of 3 mm; (b) particle size distribution.

Hertz: Elastic contact between particles is described by the Hertz law. If $\Delta^{mn} < \Delta_e$, the elastic contact force is

$$\frac{F^{mn}}{\pi R^2} = \frac{4E}{3\pi}\left(\frac{\Delta^{mn}}{R}\right)^{\frac{3}{2}}, \tag{34}$$

where R and E are the equivalent radius and the equivalent modulus of the contact, defined as

$$\frac{1}{R} = \frac{1}{r_m} + \frac{1}{r_n}, \qquad \frac{1}{E} = \frac{1-\nu_m^2}{E_m} + \frac{1-\nu_n^2}{E_n}. \tag{35}$$

Δ_e is the cutoff that separates elastic contact from plastic.

Similarity solution: The elastic regime only applies at the very early stage of compaction when particle deformation is small. Plastic deformation quickly eclipses the elastic one and dominates the compaction. If the elastoplastic response of the solid particle can be described as a linear elastic followed by a power-law plastic response, characterized by a hardening exponent α, the total strain responds to the applied stress

$$\epsilon_i = \begin{cases} \sigma/E_i & \sigma \le \sigma_{yi} \\ (\sigma/\sigma_i)^{\alpha_i} & \sigma > \sigma_{yi} \end{cases}, \tag{36}$$

where the index $i = m, n$ refers to the particles coming in contact and σ_{yi} are the reference yielding stresses. The continuity of the response at $\sigma = \sigma_{yi}$ provides the relation

$$\sigma_i = \sigma_{yi} \sqrt[\alpha_i]{\frac{E_i}{\sigma_{yi}}} \tag{37}$$

to compute the reference yielding stress from the engineering counterpart. There is no general solution to compute the interaction between two dissimilar particles when the contact is in the elastoplastic regime. An approximate solution, "similarity solution", is available if the hardening coefficients of both particles coming into

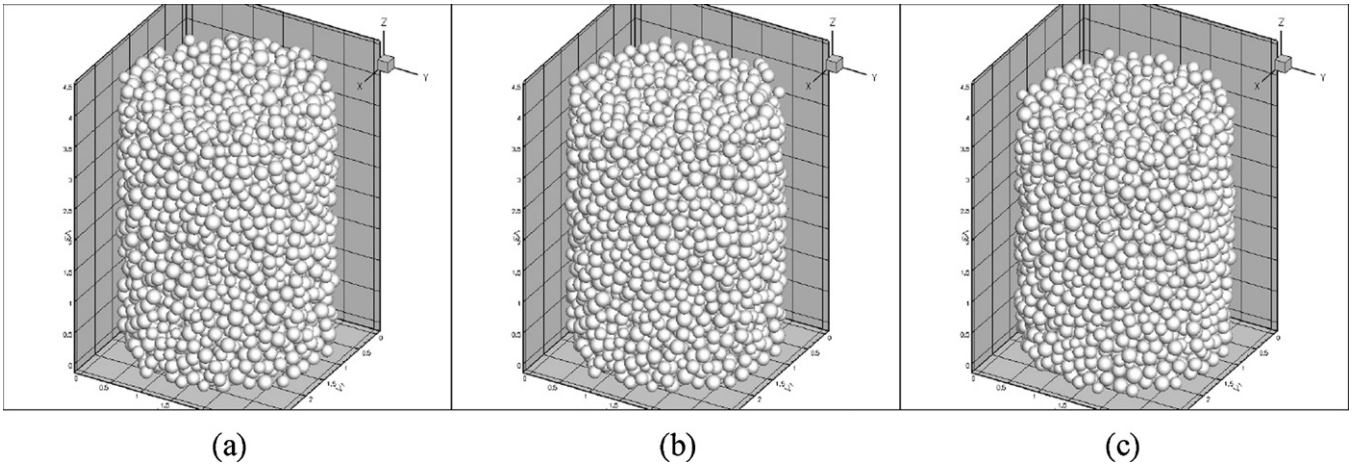

Fig. 2. Configuration of granular bed with (a) slight; (b) moderate and (c) extensive particle rearrangement. The relative bulk density is 0.545, 0.576 and 0.611 in (a), (b) and (c) respectively.

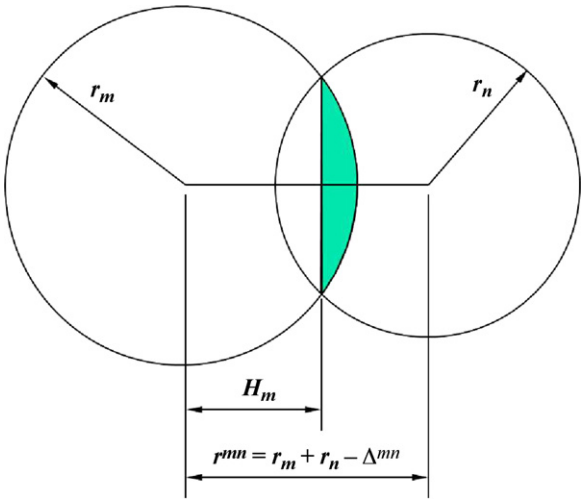

Fig. 3. Schematic diagram of inter-particle contant and nomenclature.

contact are close. Let $\alpha_m \approx \alpha_n = \alpha$, the estimated interaction provided by Storakers et al. (1999) is expressed as

$$\frac{F^{mn}}{\pi R^2 \Gamma} = B(\alpha)\left[2c^2(\alpha)\right]^{(1+1/2\alpha)} k(\alpha) \cdot \left(\frac{\Delta^{mn}}{R}\right)^{1+(1/2\alpha)}, \tag{38}$$

where the equivalent reference stress Γ is defined

$$\frac{1}{\Gamma^\alpha} = \frac{1}{\sigma_1^\alpha} + \frac{1}{\sigma_2^\alpha}, \tag{39}$$

in a similar way as the equivalent radius and the equivalent Young's modulus of the contact. The coefficients $c(\alpha)$, $k(\alpha)$ and $B(\alpha)$ in Eq. (38) are the functions (only of the hardening parameter), which are rebuilt to follow

$$c^2(\alpha) = 1.5 - \frac{1}{\sqrt{\alpha}}, \quad k(\alpha) = 3.07 \times \sqrt[\alpha]{0.16},$$

$$B(\alpha) = \begin{cases} 0.74 + 0.26/\alpha & \alpha < 3, \\ 0.64 + 0.57/\alpha & \alpha \geq 3. \end{cases}$$

from the curves supplied in Storakers et al. (1999). To test the applicability of the similarity solution to particle systems, two limit cases – that of elastic and ideal plastic, corresponding to $\alpha = 1$ and ∞, respectively, are recovered. Substituting $\alpha = 1$ and noting that $\sigma_i = E_i$ in this case, the similarity solution (38) approximately recovers the Hertzian law, of which there exists ample experimental validation for the elastic regime. In the case of $\alpha = \infty$, a linear dependency is predicted by (38) which is in good agreement with the recent experiments of Naito et al. (1998) for nearly ideal plastic materials. Therefore, we have enough reasons to believe the similarity solution can adequately address the plastic contact problem when the material is described by a power-law (36).

The ability of the quasi-continuum formulation to replicate the theoretical results based on the contact of two equi-sized spheres has been verified using the regular cubic packings shown in Fig. 4(a) and (b). For the purposes of these simulations, a mesh composed of 12-node prism elements was utilized. Its parallel surfaces are triangular and interpolated quadratically using 6 nodes (3 corner and 3 mid-side nodes). Once the mesh is generated, particles are assigned to their corresponding elements. A particle belongs to a given element if its centroid is contained within the elemental volume. If the centroid lies exactly on the boundary between two adjacent elements, the particle can be assigned to either element. The mesh shown in the figures has been chosen to maintain the same number of contacts per unit length as in the theoretical computations of bi-particle contact. The well-developed framework of finite elements can be readily applied for different boundary conditions, such as rigid punch, flexible punch or anything in between. For the purposes of our simulations, conditions representing a rigid punch and a frictionless container wall were selected, due to the particles being much softer than the die. Friction between the granular particles and between particles and the container wall plays an important role in the compaction of powder beds, however it was neglected at this stage of the development of the model this work. Fig. 5(a) shows the macroscopic normal stress on the bed as a function of the strain for a large value of the hardening exponent ($\alpha = 10$), corresponding to plastic behavior. The elastic case is similarly recovered for $\alpha = 1$, as shown in Fig. 5(b). It can be seen that the results yielded by the quasicontinuum model are in perfect agreement with those suggested by the analytical solutions.

The fundamental assumption of the similarity solution is that the contact must be local, i.e. no interference from other contacts with the same particle. This may present an obstacle for its application for systems such as the one considered here, because each of the particles in the granular bed may be surrounded by many other particles. In other words, there may be many contacts occurring simultaneously with the same particle. Fortunately, Storakers et al. (1999) has demonstrated that the similarity solution validates up to 40% of deformation without need to worry about multi-contact interaction, which effectively covers the deformation from the elastoplastic to the fully plastic regime. It should be noted that the overall accuracy of single-contact models has been shown to diminish for compaction to over 80% of the theoretical density (particle density). Any results shown here exceeding that limit have been presented for reasons of completeness.

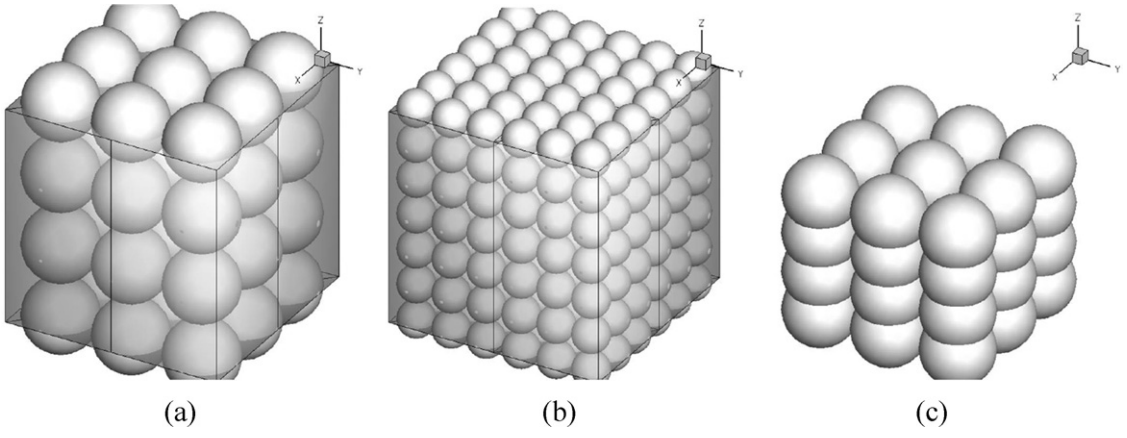

Fig. 4. Compression of regular cubic arrangements of spherical particles of uniform size. (a) $3 \times 3 \times 3$ arrangement and mesh, (b) $6 \times 6 \times 6$ arrangement and mesh, (c) $3 \times 3 \times 3$ configuration – compressed.

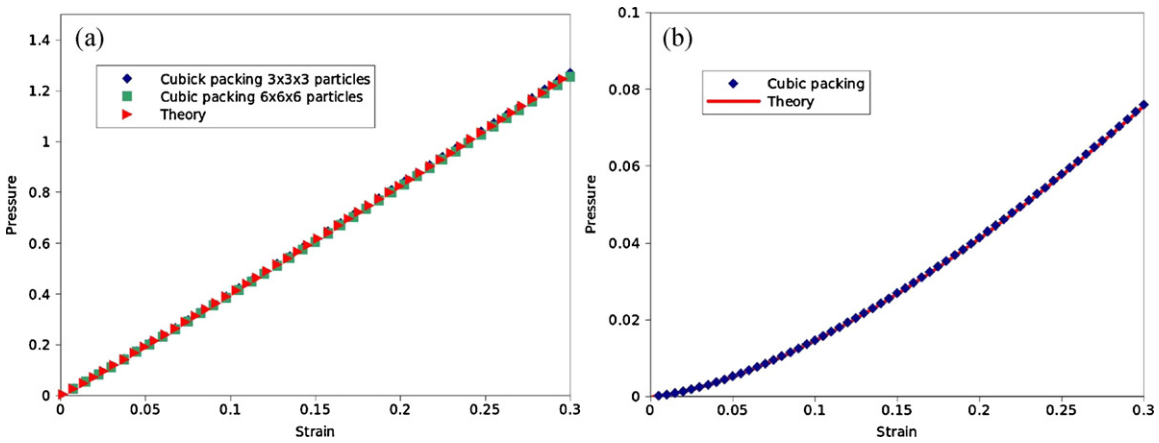

Fig. 5. Comparison of bed compression simulation results with theory: (a) plastic deformation, (b) elastic deformation.

The lower limit of the similarity solution is at Δ_e where it crosses with Hertz law. The continuity of the contact force at this point gives rise to

$$\Delta_e = \left[\frac{3\pi\Gamma}{4E}B(\alpha)k(\alpha)\right]^{(2\alpha)/(\alpha-1)}\left[2c^2(\alpha)\right]^{(\alpha+1)/(\alpha-1)} \tag{40}$$

where $\alpha \neq 1$, otherwise the Hertz law is always applicable. The upper limit of the similarity solution is the point, beyond which the contact is in the large deformation regime, where inter-particle interaction is no longer only a contact problem. At this point, the effects of a solidified material must be considered. Fig. 6 shows the elasto-plastic behavior of a random-packed bed. Different curves correspond to different ratios of the yielding stress σ_{yi} and the Young's modulus, E. The bed response ranges from almost purely elastic (at high values of the yielding stress) to almost entirely plastic (for cases where yield occurs at very low loadings), and spans the full range of intermediate behavior in between. All compression simulations shown have been carried out for a hardening exponent value of 10.

Particle–particle bonding: In order to endow the compacted solid with a tensile strength, bonding between individual particles is considered to occur in cases of finite contact areas. We introduce a phenomenological expression that correlates the evolving bonding strength s_0^{mn} between two contacting particles m and n to the current maximum of distribution of normal compressive stresses at the contact zone, which is denoted by p_0^{mn}. More precisely, we consider that

$$s_0^{mn} = c_b p_0^{mn}, \tag{41}$$

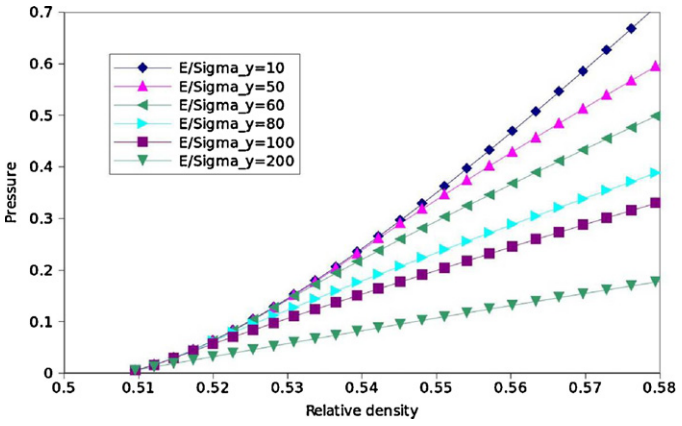

Fig. 6. Stress–strain curves, corresponding to the loading of a random-packed bed for different values of the particle yielding stress.

where the constant c_b is obtained from calibration using experimental results. Note that since p_0^{mn} depends on the degree of inter-particle compression, which is generally different for each individual contact pair, s_0^{mn} is also dependent upon the local consolidation conditions, and thus, the overall compact strength is obtained as the addition of the individual contributions of each particle–particle bonding along the failure (weakest) path. Maps of particle–particle bonding are shown in Fig. 7, which shows that not only the bonding is *heterogenous* (changing from point to point) but also *anisotropic* (direction dependent). Anisotropic properties of pharmaceutical solids have previously been reported by Heng et al. (2006). The bonding directionality, as schematically shown in Fig. 8, leads to a solid with local strength texture, therefore, the overall tensile strength is dependent on the tensile loading direction.

Tensile regime: The tensile strength developed during the consolidation process due to particle–particle bonding is exercised when a reversal of the load is imposed. The tensile regime is generally characterized by

$$\tilde{\Delta}^{mn} = \Delta^{mn} - \left(\Delta^{mn}_{\max} - \Delta^{mn}_{\text{elastic}}\right) < 0, \tag{42}$$

where

$$\Delta^{mn}_{\text{elastic}} = R\left(\frac{3}{4}\frac{F^{mn}_{\max}}{ER^2}\right)^{\frac{2}{3}}$$

is the overlap reduction during the elastic unload, and $\Delta^{mn}_{\max}$ and $F^{mn}_{\max}$ are the maximum overlapping and maximum compressive force attained during consolidation, respectively. Note that if the yield stress is not exceeded during compression (elastic regime), then $\Delta^{mn}_{\text{elastic}} = \Delta^{mn}_{\max}$, and thus, $\tilde{\Delta}^{mn} = \Delta^{mn}$.

In the tensile regime, the inter-particle *tensile* force between particles m and n is determined by following expression

$$F_b^{mn} = \pi R^2 s_0^{mn} e^{(\tilde{\Delta}^{mn}/R)}, \tag{43}$$

which provides a gradual reduction of the available tensile force with the effective inter-particle separation, given by (42), once the inter-particle tensile strength, defined by (41), is exceeded.

5.1. Uniaxial compaction simulations

After the initial configuration of the granular bed is obtained, either by numerical simulations – the present case – or by extracting data directly from experiments, a mesh needs to be designed. For the purposes of the simulations described in this work, a mesh composed of 12-node prism elements was utilized. Its parallel surfaces are triangular and interpolated quadratically using 6 nodes (3 corner and 3 mid-side nodes). A sample mesh super-imposed over a powder bed is shown in Fig. 9.

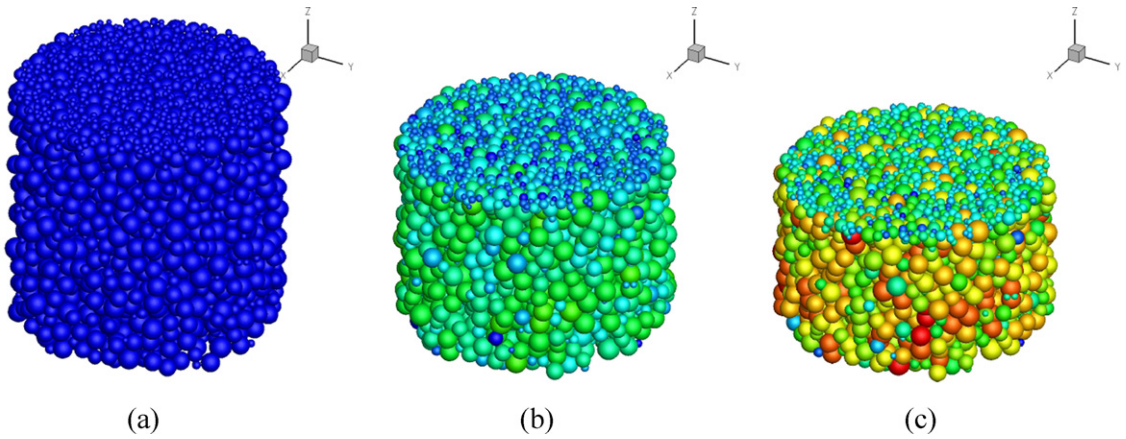

Fig. 7. Map of particle bonding forces (a) uncompacted bed; (b)intermediate compaction; (c) maximum compaction. Colors red (high) to blue (low) represent the average intensity of the bond at a given particle, which is computed by scalar addition of all bonding forces from neighboring particles and divided by the non-zero contacts. (For interpretation of the references to color in this figure legend, the reader is referred to the web version of the article.)

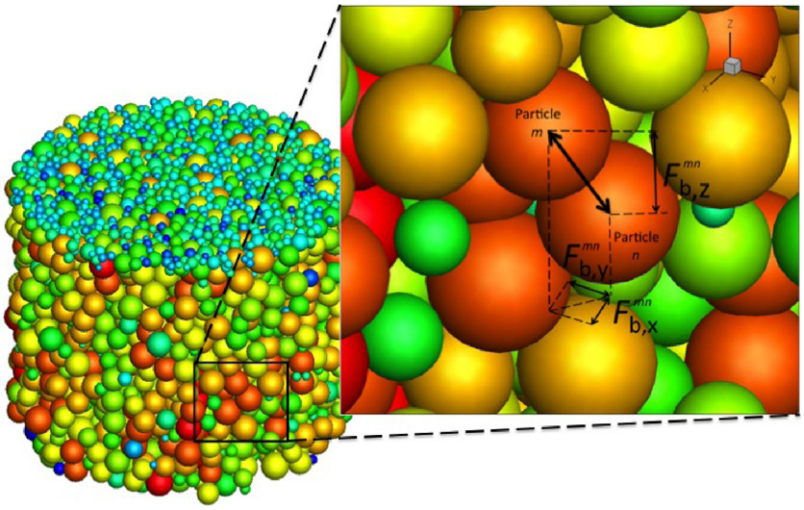

Fig. 8. Directionality of bonding force between generic particles m and n. $F_{b,i}^{mn}$ represents the bonding force between these two particles in the direction i.

Once the mesh is generated, particles are assigned to their corresponding elements. A particle belongs to a given element if its centroid is contained within the elemental volume. If the centroid lies exactly on the boundary between two adjacent elements, the particle can be assigned to either element. The well-developed framework of finite elements can be readily applied for different boundary conditions, such as rigid punch, flexible punch or anything in between. For the purposes of our simulations, conditions representing a rigid punch and a frictionless container wall were selected, due to the particles being much softer than the die. The model is predicated on the assumption that the constituent particles undergo only affine deformation as prescribed by the macroscopic strain and experience no local rearrangement in the compaction stage (the particle rearrangement stage does include inter-particle friction). This is a typical assumption for micromechanical models such as Storakers et al. (1999). While this assumption is partially justified when applied to a post-rearrangement bed, in which the large void structures have been removed, there exists evidence that inter-particle friction can have a noticeable impact on compaction even at high relative densities. An analysis of this impact can be found in Redanz and Fleck (2001). Implementation of wall friction would be straight-forward in this formulation, however, it has not been included for the generation of the results presented herein. In an attempt to replicate this condition, the physical die-wall has been lubricated using a suspension of MgSt.

The compaction of a powder bed consisting of particles with properties selected to match those of Avicel PH102 has been simulated. The mean size, density, Young's modulus, yield stress and Poisson's ratio of the modeled particles are outlined in Table 1. Values for these parameters were obtained from Roberts et al. (1994) for the Poisson ratio and Kachrimanis and Malamataris (2004) for the Young's modulus (obtained from zero-porosity compacts). For validation purposes, the values of the pressure exerted on the bed at different upper punch positions are compared to experimental data. Experimental compaction of Avicel PH102 have been carried out on the Presster a compaction emulator manufactured by MCC (Metropolitan Computing Corporation). The Presster is a compaction device, in which a moving stage equipped with standard B-tooling is propelled along a linear track, equipped with pre-compression and compression rolls, as well as an ejection cam and

Table 1
Granular Material Properties.

Name	$\overline{d}$ (μm)	ρ_s (g/cm^3)	E (MPa)	σ_y (MPa)	ν
Simulated material	100	1.6	4300	0.0475	0.3

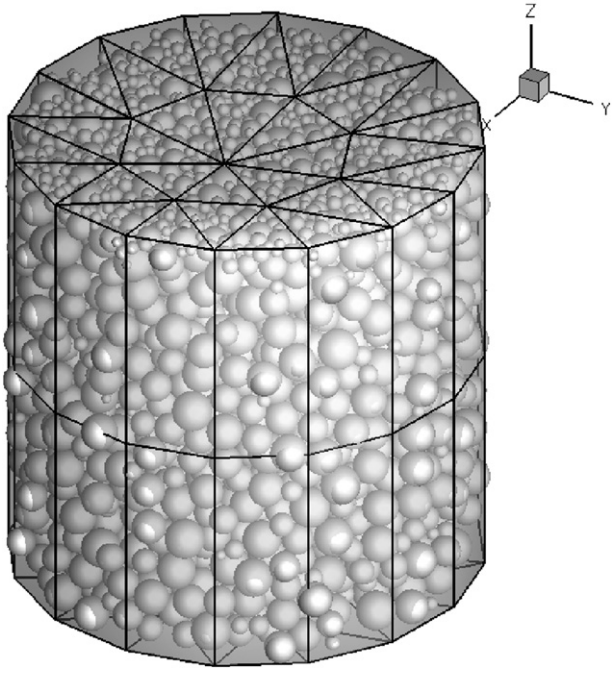

Fig. 9. Mesh super-imposed over a sample powder bed.

a take-off bar, allowing to emulate the operation of a wide range of commercially available rotary tablet presses. The compression stage is instrumented to measure pre-compression, compression, ejection, take-off and die-wall forces, punch displacement and press speed. Feeding of powder in the die is achieved by virtue of a vibratory gravity force feed shoe mechanism. In order to replicate the frictionless conditions considered in the simulations, prior to compression, the punch and die surfaces were sparingly lubricated with magnesium stearate suspended in ethanol (5%, w/v). A standard flat face 10 mm round TSM B-tooling has been used. Compaction was carried out under conditions matching the operation of a 10-station Mendel rotary press with an achieved dwell time of 29 ms.

The axial compression stress vs. strain curves are compared against experimental data in Fig. 10(a). For the purposes of this simulation a loosely packed numerical bed was generated with an initial relative density of 0.4. After rearrangement that value was increased to 0.46) The initial (after filling) relative density in the Presster die is around 0.3. In order to match the simulated bed, the powder in the Presster die is subjected to a pre-compression load. This load, however, results in a certain particle deformation, in addition to rearrangement. In order, to replicate this effect, the numerical bed is also loaded and unloaded (shown in Fig. 10(b). Once the two powder bed configurations have been brought to equal initial relative densities they are compressed to a relative density of around 0.85. The experimental and numerical compaction results are represented by the blue and red curves, respectively (Fig. 10(a)). The two curves exhibit good agreement until the late stages of compaction, above strain values of 0.3 (corresponding to a relative density of 0.8). The two curves exhibit good agreement until the late stages of compaction, above strain values of 0.3 (corresponding to a relative density of 0.8). At this point, significant interaction among contacts commences to have an effect which accounts for the rapid stiffening observed during the experiments. Fig. 11 shows the progress of the bed configuration during the process of compaction, with its un-compacted state, state in mid-compaction and fully compacted state shown in (a), (b), and (c), respectively.

5.1.1. Bonding

The compaction of a closely-packed bed proceeds by virtue of particle deformation. It is this deformation, which accounts for the increase in contact area between adjacent particles and their subsequent bonding via various surface forces. This process is replicated in the numerical model by assigning a bonding force acting between each pair of particles in contact. The force is a function of the maximum inter-particle pressure p_0^{mn}, in accordance to Eq. (43). Fig. 12 shows the compression force versus displacement curves corresponding to the compaction, relaxation and subsequent tensile loading of a powder bed (multiple compaction forces are represented). The bonding force formulation is calibrated using experimental tablet tensile loading results. The procedure used for calibration was the following. A tablet was produced at a compaction pressure in the middle of the studied range using the Presster. This tablet was then subjected to a tensile load until failure and the corresponding force was recorded. A numerical simulation was performed matching the experimental conditions as closely as possible. The parameter c_b was then varied until the failure of the numerically simulated compact occurred at the same tensile

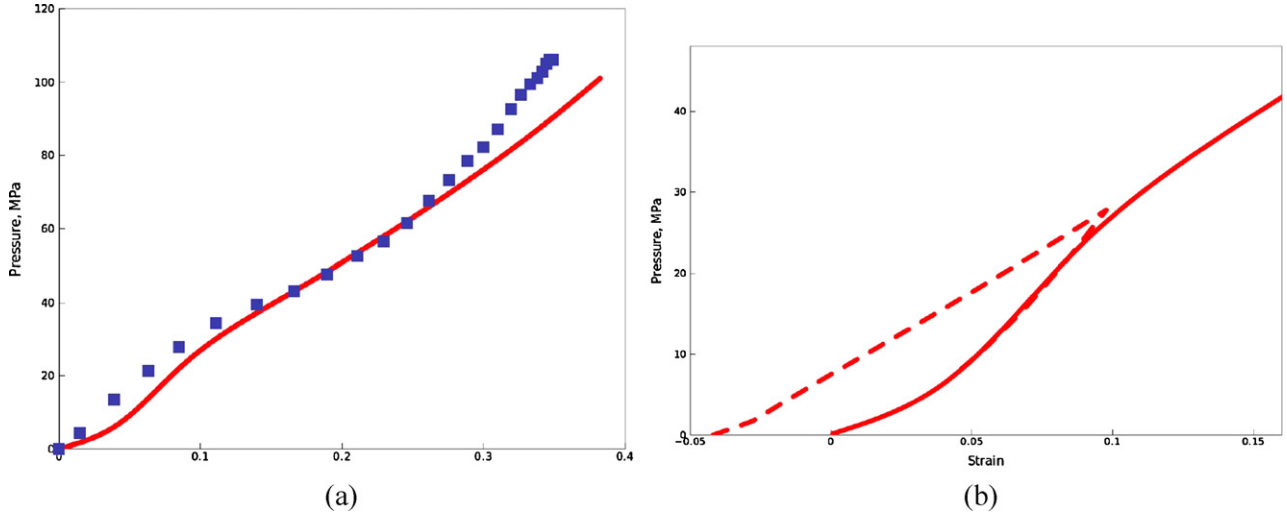

Fig. 10. Pressure vs. strain, (a) comparison of numerical (red curve) and experimental (blue symbols) results; (b) close-up of the unload–reload portion of the curve generated by the numerical simulation (shown by the dashed (- - -) line). (For interpretation of the references to color in this figure legend, the reader is referred to the web version of the article.)

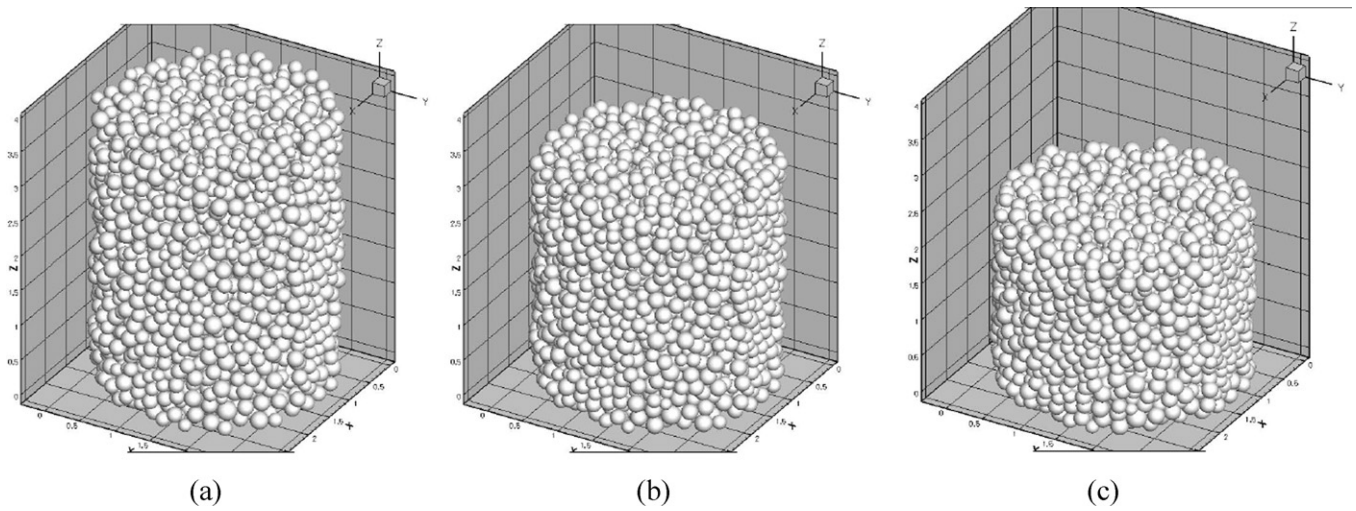

Fig. 11. Configuration of granular bed (a) before compaction; (b) during compaction and (c) in its densest state.

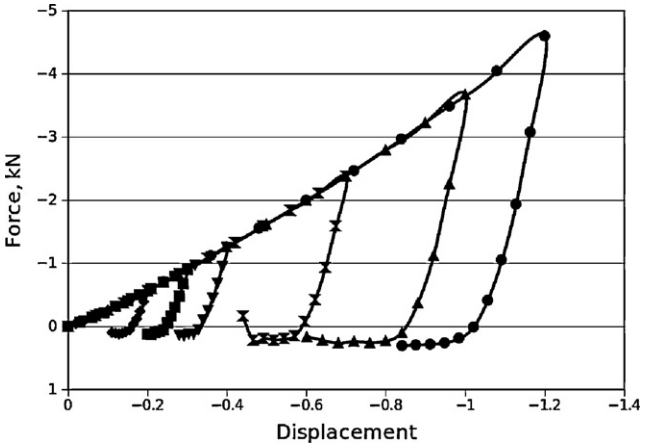

Fig. 12. Compression, relaxation and tensile loading of powder beds.

load as the physical tablet. The value of c_b, thus obtained, was used for all subsequent simulations. The maximum tensile stress achieved corresponds to tensile strength of the material. A post-failure behavior is also observed in our simulations due to: (i) the smooth inter-particle force decay of potentials provided in Eq. (43) and (ii) the imposed displacement boundary conditions applied. It should be noted this post-failure regime is unstable under force-controlled conditions, resulting in an immediate failure after the tensile strength has been reached. Each tensile loading curve in Fig. 12 exhibits a part of steep increase, followed by a decay tail. Of these, only the first part is significant for estimating tablet strength. The peak tensile stress is treated as a mark of tablet failure. In the numerical system, individual particles debond gradually during the tensile loading, with the axial stress going through a local maximum before starting to decay. This is the stage where crack propagation is initiated. The method in its current implementation is not equipped to simulate discrete fracture behavior and the post-failure behavior is therefore mesh size dependent (hence the dismissal of the subsequent portion of the loading curve). In the graph, compression corresponds to negative forces and displacements, and tension is described by positive values.

For the purposes of validation of the model, tablet compression has been carried out both physically (in the Presster) and numerically, while keeping the process parameters and materials properties as similar as possible. The physical tablets have been subjected to tensile loads through the use of a device especially designed for the purpose. The device consists of two linear stepper motors positioned along the same axis. A metal plate was attached to each stepper motor. After gluing the flat faces of a tablet to each metal plate, the stepper motors can be used pull on the tablet along their common axis, which passes through the centerline of the tablet. Load cells mounted on the holder plates were used to measure the resulting force. To account for the compliance of the tensile tester the two metal plates were adhered to each other with no tablet being present. A tensile stress was then applied up to the value of the highest fracture force obtained from the MCC tablets. The force/displacement curve was then subtracted from the measured force/displacement curves obtained from the tablets. Fig. 13 shows the values of the break force for tablets, e.g.

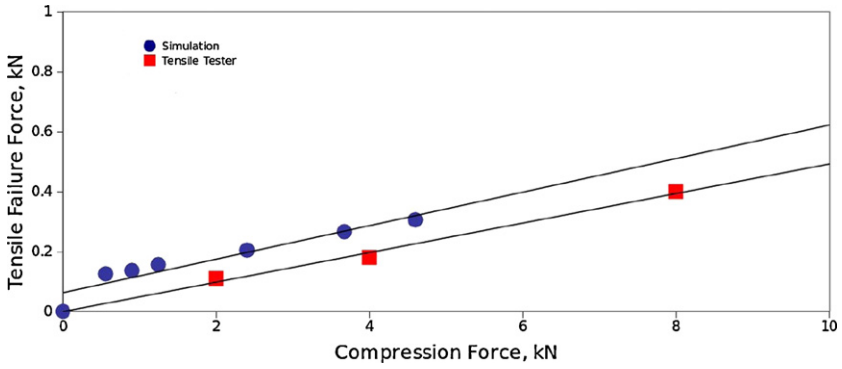

Fig. 13. Tablet tensile strength as a function of the compaction force.

the applied tensile force, at which the tablets break (both physical and simulated) as a function of the force, at which they have been compressed. There is a reasonably good agreement between the numerical and experimental results, with a small overshoot by the numerical values, caused by the tail of the bonding force distance decay formulations (expressions involving a cut-off distance caused the simulations to become unstable). It is noteworthy that despite predicting slightly higher values for the tablet tensile strengths, the model manages to reproduce the slope of the curve to a large degree.

6. Conclusions

A quasi-continuum numerical method has been implemented to study the compaction of granular beds. The technique resolves the bed on the particle level, using particle–particle interactions to calculate the deformation of the FEM mesh discretizing the domain. Simulations of the compaction of Avicel PH102 demonstrate the ability of the model to replicate the compaction behavior of physical systems. The ability of the method to incorporate local inter-particle forces, has been used to simulate the consolidation of a granular assembly, in which bonding forces form between neighboring particles as a function of contact area. A generic expression for the strength of the bonds, calibrated using experimental data has been shown to be able to predict the tensile strength of tablets composed of a pharmaceutical excipient to a reasonable degree.

Acknowledgments

This material is based upon work supported by the National Science Foundation under Grant ECE-0540855.

References

Aydin, I., Briscoe, B., Sanliturk, Y., 1996. The internal form of compacted ceramic components: a comparison of finite element modeling with experiment. Powder Technol. 89, 239–254.
Bhatia, R., Lordi, N., 1979. Electrical conductance of directly compressible materials under pressure. J. Pharm. Sci. 68, 222–226.
Boer, A.D., Bolhuis, G., Lerk, C., 1978. Bonding characteristics by scanning electron microscopy of powders mixed with magnesium stearate. Powder Technol. 20, 75–82, URL http://www.sciencedirect.com/science/article/B6TH9-442B8RG-KP/2/d69d6f0ecf9a6730c9cae5e9bfa4bab3.
Borja, R.I., Lee, S., 1990. Cam-clay plasticity, part i: implicit integration of elasto-plastic constitutive relations. Comp. Methods Appl. Mech. Eng. 78, 49–72.
Chang, W., Etsion, I., Bogy, D., 1987. J. Tribol. 110, 1–7.
Cocks, A., Sinka, I., 2007. Constitutive modeling of powder compaction - i. Theoretical concepts. Mech. Mater. 39, 392–403.
Dec, R.T., Zavaliangos, A., Cunningham, J.C., 2003. Comparison of various modeling methods for analysis of powder compaction in roller press. Powder Technol. 130, 265–271.
Derjaguin, B., Muller, V., Toporov, Y., 1975. J. Colloid Interface Sci. 53, 314–326.
DiMaggio, F.L., Sandler, I.S., 1971. Material model for granular soils. J. Eng. Mech. ASCE 96, 935–950.
Drucker, D.C., Prager, W., 1952. Soil mechanics and plastic analysis of limit design. Q. Appl. Math. 10, 157–165.
Dvorkin, E., Cuitino, A., Gioia, G., 1989. A concrete material model based on non-associated plasticity and fracture. Eng. Comput. 6, 281–294.
Fleck, N., 1995. On the cold compaction of powders. J. Mech. Phys. Solids 43, 1409–1431.
Fleck, N., Storakers, B., McMeeking, R., 1997. The viscoplastic compaction of powders. In: Fleck, N., Cocks, A. (Eds.), Mechanics of Granular and Porous Materials. Kluwer, pp. 1–10.
Fleck, N.A., Kuhn, L.T., Meeking, R.M., 1992. Yielding of metal powder bonded by isolated contacts. J. Mech. Phys. Solids 40, 1139–1162.
Gilabert, F., Quintanilla, M., Castellanos, A., Valverde, J., 2007. Adhesive elastic plastic contact: theory and numerical simulation. ZAMM – Z. Angew Math. Mech. 87, 128–138.
Gioia, G., Cuitiño, A., Zheng, S., Uribe, T., 2002. Two-phase densification of cohesive granular aggregates. Phys. Rev. Lett. 88, 204302:1–4.
Gurson, A.L., 1977. Continuum theory of ductile rupture by void nucleation and growth: Part i - yield criteria and flow rules for porous ductile media. J. Eng. Mater. Tech. 99, 2–15.
Heckel, R., 1961. Density–pressure relationship in powder compaction. Trans. Metall. Soc. AIME 221, 671–675.
Heng, J., Bismarck, A., Lee, A., Wilson, K., Williams, D., 2006. Anisotropic surface energetics and wettability of macroscopic form i paracetamol crystals. Langmuir 22, 2760–2769.
Heyliger, P.R., McMeeking, R.M., Sep. 2001. Cold plastic compaction of powders by a network model. J. Mech. Phys. Solids 49, 2031–2054.
Jerier, J.-F., Hathong, B., Richefeu, V., Chareyre, B., Imbault, D., Donze, F.-V., Doremus, P., 2011. Study of cold powder compaction by using the discrete element method. Powder Technol. 208 (2), 537–541.
Johnson, K., Kendall, A., Roberts, A., 1971. Proc. R. Soc. London 324, 301–313.
Jullien, R., Meakin, P., 1988. Ballistic deposition and segregation of polydisperse spheres. Europhys. Lett. 6, 629–634.
Jullien, R., Meakin, P., 1989. Simple-models for the restructuring of three-dimensional ballistic aggregates. J. Colloid Interface Sci. 127, 265–272.
Kachrimanis, K., Malamataris, K., 2004. "Apparent" young's elastic modulus and radial recovery for some tableted pharmaceutical excipients. Eur. J. Pharm. Sci. 21, 197–207, URL http://www.sciencedirect.com/science/article/B6T25-4B8BXPN-6/2/54937bbe5c3fea096956dff5cb0a6b89.
Kadin, Y., Kligerman, Y., Etsion, I., 2008. Loading-unloading of an elastic–plastic adhesive spherical microcontact. J. Colloid Interface Sci. 321, 242–250.
Kadiri, M., Michrafy, A., Dodds, J., Sep. 2005. Pharmaceutical powders compaction: experimental and numerical analysis of the density distribution. Powder Technol. 157, 176–182.
Kawakita, K., Ludde, K., 1970. Some considerations on powder compression equations. Powder Technol. 4, 61–68.
Khoei, A., Shamloo, A., Azami, A., 2006. Extended finite element method in plasticity forming of powder compaction with contact friction. Int. J. Solids Struct. 43, 5421–5448 (September).
Kogut, L., Etsion, I., 2003. J. Colloid Interface Sci. 261, 372–378.
Kuhn, H., Downey, C., 1973. Material behaviour in powder preform forging. J. Eng. Mater. Technol. 18, 41–46.
Martin, C.L., Bouvard, D., 2003. Study of the cold compaction of composite powders by the discrete element method. Acta Mater. 51, 373–386.
Maugis, D., 1992. J. Colloid Interface Sci. 150, 243–269.
Maugis, D., Pollock, H., 1984. Acta Metall. 32, 1323–1334.
Michrafy, A., Ringenbacher, D., Tchoreloff, P., 2002. Modeling the compaction behavior of powders: application to pharmaceutical powders. Powder Technol. 127, 257–266.
Muller, V., Yuschenko, B., Derjaguin, B., 1980. J. Colloid Interface Sci. 77, 91–101.
Naito, M., Nakahira, K., Hotta, T., Ito, A., Yokoyama, T., Kamiya, H., 1998. Microscopic analysis on the consolidation process of granule beds. Powder Technol. 95, 214–219.
Oda, M., Iwashita, K., Oct. 2000. Study on couple stress and shear band development in granular media based on numerical simulation analyses. Int. J. Eng. Sci. 38, 1713–1740.
Olsson, H., Adolfsson, A., Nystrom, C., 1996. Compaction and measurement of tablets in liquids with different dielectric constants for determination of bonding mechanisms–evaluation of the concept. Int. J. Pharm. 143, 233–245, URL http://www.sciencedirect.com/science/article/B6T7W-3RG55WG-1H/2/9b96f050b3d219ab9a74efea20625ced.
Pavier, E., Doremus, P., 1999. Triaxial characterisation of iron powder behaviour. Powder Metall. 42, 345–352.
Pizette, P., Martin, C., Delette, G., Sornay, P., Sans, F., 2010. Compaction of aggregated ceramic powders: from contact laws to fracture and yield surfaces. Powder Technol. 198, 240–250, URL http://www.sciencedirect.com/science/article/B6TH9-4XRYT6V-2/2/36ad1d11c80e6f46236f42d4a2d897ac.
Procopio, A.T., Zavaliangos, A., Jul. 2005. Simulation of multi-axial compaction of granular media from loose to high relative densities. J. Mech. Phys. Solids 53, 1523–1551.
Redanz, P., Fleck, N.A., Dec. 2001. The compaction of a random distribution of metal cylinders by the discrete element method. Acta Mater. 49, 4325–4335.
Roberts, R., Rowe, R., York, P., 1994. The Poisson's ratio of microcrystalline cellulose. Int. J. Pharm. 105, 177–180, URL http://www.sciencedirect.com/science/article/B6T7W-4772DMY-3D/2/6c45317a2a732828481c6612c7939201.
Rodney, D., Phillips, R., 1999. Structure and strength of dislocation junctions: an atomic level analysis. Phys. Rev. Lett. 82, 1704–1707.
Adolfsson, A., Olsson, H., Nystrom, C., 1997. Effect of particle size and compaction load on interparticulate bonding structure for some pharmaceutical materials studied by compaction and strength characterisation in butanol. Eur. J. Pharm. Biopharm. 44, 243–251, URL http://www.sciencedirect.com/science/article/B6T6C-3S4Y014-3/2/f6a3223b416ba8bc77e23c0c0edf2066.
Schofield, A.N., Wroth, C.P., 1968. Critical State Solid Mechanics. McGraw-Hill, London, UK.
Shenoy, V., Phillips, R., Tadmor, E., 2000. Nucleation of dislocations beneath a plane strain indenter. J. Mech. Phys. Solids 48, 649–673.
Shima, S., Oyane, M., 1976. Plasticity theory for porous metals. Int. J. Mech. Sci. 18, 285–291.
Sinha, T., Bharadwaj, R., Curtis, J.S., Hancock, B.C., Wassgren, C., 2010. Finite element analysis of pharmaceutical tablet compaction using a density dependent material plasticity model. Powder Technol. 202, 46–54, URL http://www.sciencedirect.com/science/article/B6TH9-4YVY79F-1/2/aa8c9f754c0daec12a98212842bdb0bb.
Sinka, I.C., Cunningham, J.C., Zavaliangos, A., 2003. The effect of wall friction in the compaction of pharmaceutical tablets with curved faces: a validation study of the Drucker–Prager cap model. Powder Technol. 133, 33–43 (July).

Smith, G., Tadmor, E., Kaxiras, E., 2000. Multiscale simulation of loading and electrical resistance in silicon nanoindentation. Phys. Rev. Lett. 84, 1260–1263.
Song, J., Srolovitz, D., 2006. Acta Mater. 54, 5305–5312.
Storakers, B., Fleck, N., McMeeking, R., 1999. The viscoplastic compaction of composite powders. J. Mech. Phys. Solids 47, 785–815.
Tabor, D., 1977. J. Colloid Interface Sci. 58, 2–13.
Thornton, C., Antony, S.J., Apr. 2000. Quasi-static shear deformation of a soft particle system. Powder Technol. 109, 179–191.
Vromans, H., Lerk, C., 1988. Densification properties and compactibility of mixtures of pharmaceutical excipients with and without magnesium stearate. Int. J. Pharm. 46, 183–192, URL http://www.sciencedirect.com/science/article/B6T7W-47555SG-1JH/2/ef3ac8e79a29f4f22dfdc5efe2e4ce47.
Westwood, W.D., 1989. Reactive sputtering. Phys. Thin Films 14, 57–79.
Wu, C.-Y., Ruddy, O., Bentham, A., Hancock, B., Best, S., Elliott, J., 2005. Modelling the mechanical behaviour of pharmaceutical powders during compaction. Powder Technol. 152, 107–117 (April).
Zhang, Y., Chakrabarti, S., 2003. Physical properties and compact analysis of commonly used direct compression binders. AAPS PharmSciTech 4, 1–11.
Zheng, S., Cuitino, A., 2002. Consolidation behavior of inhomogeneous granular beds of ductile particles using a mixed discrete-continuum approach. KONA 20, 168–177.
Zuurman, K., der Voort Maarschalk, K.V., Bolhuis, G.K., 1999. Effect of magnesium stearate on bonding and porosity expansion of tablets produced from materials with different consolidation properties. Int. J. Pharm. 179, 107–115, URL http://www.sciencedirect.com/science/article/B6T7W-3VYXX77-C/2/34b84495acaeb9ff2cc087d0d7c1b530.